



DOI 10.24425/aee.2025.153012

The propagation of power line carrier communication technology in power transmission cables-circuital approach and Finite Integration Technique modeling

HAKIM AZIZI ¹✉, MOHAMMED CHEBOUT ², MOHAMMED CHARIF KIHAL ³,
DAOUD SEKKI ⁴, HOCINE MOULAI ⁵

¹*Renewable Energy Systems Applications Laboratory, Ziane Achour University
Djelfa, 17000, Algeria*

²*Applied Automation and industrial Diagnostic Laboratory, Ziane Achour University
Djelfa, 17000, Algeria*

³*Department of Electrical Engineering, Mohamed Seddik Ben Yahia University
Jijel, 18000, Algeria*

⁴*Mohamed Cherif Messaadia University
Souk Ahras, 41000, Algeria*

⁵*Laboratory of Characterization and Diagnosis of Power Equipments (LCDEP)
University of Science and Technology Houari Boumediene
Algiers, 16311, Algeria*

*e-mail: {✉ h.azizi/m.chebout}@univ-djelfa.dz,
mc.kihal@univ-jijel.dz, daoud.sekki@univ-soukahras.dz, hmoulai@usthb.dz*

(Received: 19.05.2024, revised: 31.01.2025)

Abstract: The real-time management of the Production-Transport-Consumption system reveals the need for information on the state of the network and the means of action on it at all times. This need is met through the use of telecontrol systems. These operate mainly on substations, complex installations that ensure the interconnection of lines and the transformation of voltage levels. In this work, we are interested in the propagation of Power Line Carrier (PLC) communication technology in power cables, both on a single cable and on a Y topology. We will analyze respectively the effect and the influence of several factors on the transfer function such as: effect of the end loads, the length of cable, the junction between two sections of cables in order to deduce the frequency channel of most favorable transmission. The results of the transfer function predictions obtained by the analytical formulation are compared and validated with full-field simulations using the CST software.

Key words: frequency channel, Power Line Carrier (PLC), power transmission cable, transfer function



© 2025. The Author(s). This is an open-access article distributed under the terms of the Creative Commons Attribution-NonCommercial-NoDerivatives License (CC BY-NC-ND 4.0, <https://creativecommons.org/licenses/by-nc-nd/4.0/>), which permits use, distribution, and reproduction in any medium, provided that the Article is properly cited, the use is non-commercial, and no modifications or adaptations are made.

1. Introduction

Even in today's world of high-speed internet and fiber optics, Power Line Carrier (PLC) is still widely used to provide real-time communications for protection of high voltage transmission lines [1]. PLC is often the most economical and reliable high-speed dedicated channel available for protective relaying. A power line carrier system includes three basic elements [2]: a transmission line, presenting a channel for the transmission of carrier energy; tuning, blocking, and coupling equipment, providing a means of connection to the high-voltage transmission line; transmitters, receivers, and relays. Driving an electrical system is, first of all, defining the sharing of roles and responsibilities between the many actors involved [3–5]. Then, for the “transmission system managers” who, in each country or major area of operation, have the role of conductor and the direct control of the means of conduct [6], it is a question of preparing the situations to come, then, from their control centers or “dispatching”, to monitor the system and to control it, to anticipate the possible difficulties.

In order to drive the production-transport-consumption system, reliable information must be collected at the enslaved electrical substations (points of the electricity grid) and then transmitted to the treatment centers [7–9]. The system of data transmission between the slave stations (SS) and the various control stations (CS) is an essential link in the overall remote monitoring system. Its dependability must be carefully studied: Reliable media and information transmissions in the most sensitive conditions and protection of information against different types of disturbances (pipes and radii).

The different technologies used to ensure data transmission are as follows: leased telephone lines, carrier currents on line, cables with telecommunication circuit and radio links [10]. PLC technology is nowadays the most desired for multiple advantages; the most important one is the use of the network even in charge of the transmission of electrical energy [11]. The major arteries of the electricity network are overhead lines or underground buried cables. Moreover, in the electricity grid, we are increasingly encountering the use of overhead or underground cables for the transmission of energy; these cables, originally planned technically for the routing of power frequency energy, are now more and more used to transmit low energy medium and high frequency signals [12–15].

2. Modeling the propagation of PLC in a cable network

To model the propagation of PLC in a cable network, we use the topological formalism of the type $[A][X] = [B]$ proposed by A. Amétani *et al.* [1]. This formalism applies particularly to wire structures, guaranteeing a relatively low computation time. For the elaboration of this formalism, we propose the presentation of some theoretical concepts relating to the representation of a multifilar line by matrix $[\phi]$.

2.1. Formalism of transmission lines

To model this cable by the theory of transmission lines we use the formalism proposed by A. Amétani [1]. We give the main lines of this formalism in the following subparagraphs. Consider a multi-wire line, whose return conductor is the n -th conductor as shown in Fig. 1.

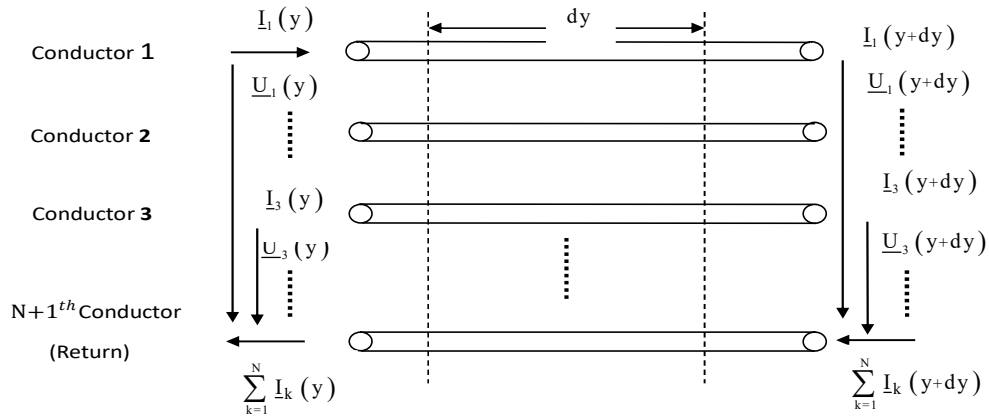


Fig. 1. Diagram of a multi-wire line

It is characterized by the following equations:

$$\begin{cases} \frac{d [\underline{U}(y)]}{dy} = - [\underline{Z}] [\underline{I}(y)] \\ \frac{d [\underline{I}(y)]}{dy} = - [\underline{Y}] [\underline{U}(y)] \end{cases}, \quad (1)$$

with: $[\underline{U}(y)]$ and $[\underline{I}(y)]$: the vectors of voltages and currents at a distance y along the cable, $[\underline{Z}]$ and $[\underline{Y}]$, respectively, the matrices (of order $N \times N$) of linear impedance and admittance of the line.

The matrices $[\underline{Z}]$ and $[\underline{Y}]$ are frequencies dependent and defined as follows:

$$[\underline{Z}] = [\underline{R}] + jw [\underline{L}], \quad (2)$$

$$[\underline{Y}] = [\underline{G}] + jw [\underline{C}]. \quad (3)$$

We recall the characteristics of these different parameters:

- Linear inductance matrix $[\underline{L}]$: characterizes the inter and intra conductor magnetic fluxes,
- Linear capacity coefficient matrix $[\underline{C}]$: characterizes the electrical energy stored in the lines of the electric field between two conductors separated by a dielectric and the conductors,
- Linear conductance matrix $[\underline{G}]$: power dissipated as heat in the dielectric characterizing the losses in the dielectric and the insulation defects,
- Linear resistance matrix $[\underline{R}]$: corresponds to the power dissipated as heat in the conductors.

2.2. Calculation of impedance and admittance matrices of a multilayer cable

2.2.1. Calculation of the impedance matrix

To carry out this work, we use, as we have previously stated, the approach developed by A. Amétani [1] which uses the formalism of transmission lines defined by the equivalent electrical circuit in Fig. 2.

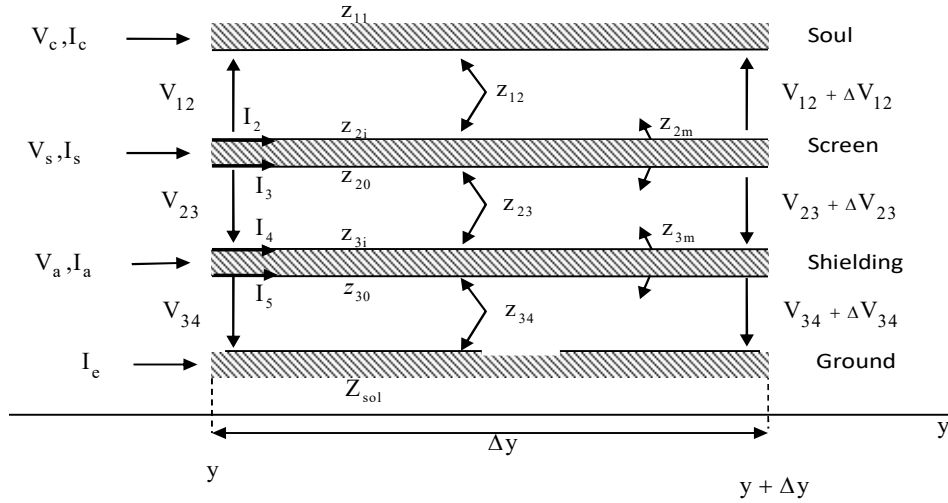


Fig. 2. Equivalent circuit of impedances

This circuit is developed [1] taking into account the different couplings between the three layers (core, screen and shields) as well as the transfer impedances of each conductive layer with:

- I_c, I_s, I_a and I_e : the currents flowing in the core, the screen, the shielding and the external environment there in y ,
- I_2, I_3, I_4, I_5 : the currents on internal and external surfaces of the screen and shield,
- V_{12}, V_{23}, V_{34} : the tensions between the soul, the screen, the shielding and the ground in y ,
- $V_{12} + \Delta V_{12}, V_{23} + \Delta V_{23}, V_{34} + \Delta V_{34}$: the tensions between the soul, the screen, the shielding, and the ground in $y + \Delta y$.

From the equivalent circuit, we have the following relations:

$$-\frac{\Delta V_a}{\Delta y} = (Z_{30} + Z_{34} - Z_{3m} + Z_0)(I_c + I_s) + (Z_{30} + Z_{34} + Z_0) I_e, \quad (4)$$

$$-\frac{\Delta V_s}{\Delta y} = (Z_{20} + Z_{23} + Z_{3i} + Z_{30} + Z_{34} - 2Z_{3m} - Z_{2m} + Z_0) I_c + (Z_{20} + Z_{23} + Z_{3i} + Z_{30} + Z_{34} - 2Z_{3m} + Z_0) I_s + (Z_{30} + Z_{34} - Z_{3m} + Z_0) I_a, \quad (5)$$

$$-\frac{\Delta V_c}{\Delta y} = (Z_{11} + Z_{12} + Z_{2i} + Z_{20} + Z_{23} + Z_{3i} + Z_{30} + Z_{34} - 2Z_{3m} - 2Z_{2m} + Z_0) I_c + (Z_{20} + Z_{23} + Z_{3i} + Z_{30} + Z_{34} - 2Z_{3m} - Z_{2m} + Z_0) I_s + (Z_{30} + Z_{34} - Z_{3m} + Z_0) I_a. \quad (6)$$

By doing $\Delta y \rightarrow 0$, we obtain

$$\frac{d[V]}{dy} = -[Z][I], \quad (7)$$

with:

- the voltage vector

$$[V] = \begin{bmatrix} V_c \\ V_s \\ V_a \end{bmatrix}, \quad (8)$$

– the current vector

$$[\underline{I}] = \begin{bmatrix} I_c \\ I_s \\ I_a \end{bmatrix}. \quad (9)$$

$$[\underline{Z}] = [\underline{Z}_{\text{inter}}] + [\underline{Z}_{\text{sol}}], \quad (10)$$

with

$[\underline{Z}_{\text{inter}}]$: matrix of the specific parameters of the internal conductors of a cable relative to the shielding which surrounds it,

$[\underline{Z}_{\text{sol}}]$: matrix which takes into account the influence of the environment external to the cable.

The matrix $[\underline{Z}_{\text{inter}}]$ is defined as follows:

$$[\underline{Z}_{\text{inter}}] = \begin{bmatrix} \underline{Z}_{cc} & \underline{Z}_{cs} & \underline{Z}_{ca} \\ \underline{Z}_{cs} & \underline{Z}_{ss} & \underline{Z}_{sa} \\ \underline{Z}_{ca} & \underline{Z}_{sa} & \underline{Z}_{aa} \end{bmatrix}, \quad (11)$$

with

$$Z_{cc} = Z_{11} + Z_{12} + Z_{2i} + Z_{20} + Z_{23} + Z_{3i} + Z_{30} + Z_{34} - 2Z_{3m} - 2Z_{2m}, \quad (12)$$

$$Z_{ss} = Z_{20} + Z_{23} + Z_{3i} + Z_{30} + Z_{34} - 2Z_{3m}, \quad (13)$$

$$Z_{aa} = Z_{30} + Z_{34}, \quad (14)$$

$$Z_{cs} = Z_{20} + Z_{23} + Z_{3i} + Z_{30} + Z_{34} - 2Z_{3m} - Z_{2m}, \quad (15)$$

$$Z_{ca} = Z_{30} + Z_{34} - Z_{3m}, \quad (16)$$

$$Z_{sa} = Z_{ca} = Z_{30} + Z_{34} - Z_{3m}, \quad (17)$$

where:

Z_{cc} is the self-impedance of the soul,

Z_{ss} is the screen's own impedance,

Z_{aa} is the shielding self-impedance,

Z_{cs} is the mutual impedance between the core and the screen,

Z_{ca} is the mutual impedance between core and shield,

Z_{sa} is the mutual impedance between screen and shield.

Z_{cc} , Z_{ss} , Z_{aa} , Z_{cs} , Z_{ca} , Z_{sa} depend on physical and geometric parameters.

2.2.2. Calculation of the admittance matrix

The internal admittance matrix (the reference being the external layer) of a single-core cable is evaluated from the matrix of potential coefficients, we have:

$$[Y] = j\omega [P^{-1}], \quad (18)$$

with $[P]$ as the matrix of potential coefficients.

For a single-core cable consisting of a core, a screen, and a shield, the equivalent electrical circuit of the admittances is given in Fig. 3.

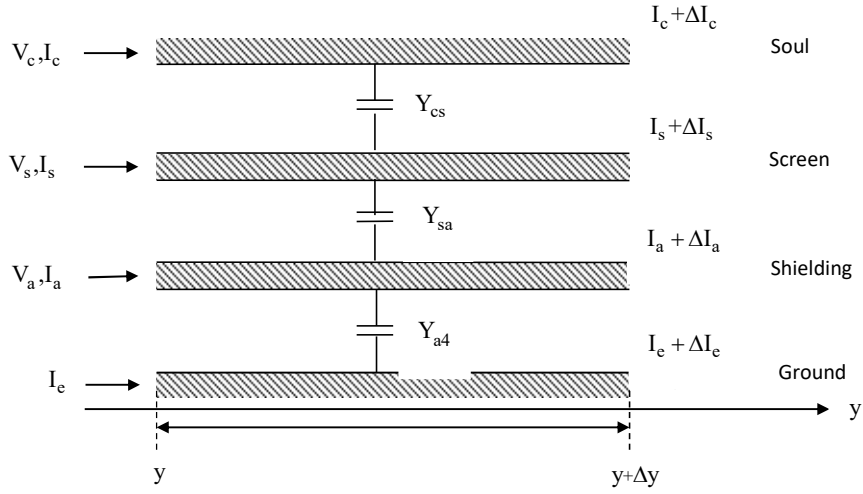


Fig. 3. Equivalent electrical circuit of the admittances of a portion of length Δy

Using Kirchhoff's relations on currents, we have:

$$-\frac{\Delta I_c}{\Delta y} = Y_{cs} V_c - Y_{cs} V_s, \quad (19)$$

$$-\frac{\Delta I_s}{\Delta y} = Y_{cs} V_c + (Y_{sa} + Y_{cs}) V_s - Y_{sa} V_a, \quad (20)$$

$$-\frac{\Delta I_a}{\Delta y} = Y_{sa} V_s + (Y_{a4} + Y_{sa}) V_a. \quad (21)$$

By writing the limit of these last three equations when Δy tends to 0, we deduce the following matrix system:

$$\frac{d}{dy} \begin{bmatrix} I_c \\ I_s \\ I_a \end{bmatrix} = - \begin{bmatrix} Y_{cs} & -Y_{cs} & 0 \\ -Y_{cs} & (Y_{sa} + Y_{cs}) & -Y_{sa} \\ 0 & -Y_{sa} & (Y_{a4} + Y_{sa}) \end{bmatrix} \begin{bmatrix} V_c \\ V_s \\ V_a \end{bmatrix} = - [\underline{Y}_i] [\underline{V}], \quad (22)$$

with:

$$Y_{cs} = \left(\frac{j\omega 2\pi \epsilon_0 \epsilon_{i1}}{\ln \left(\frac{r_3}{r_2} \right)} \right), \quad (23)$$

$$Y_{sa} = \left(\frac{j\omega 2\pi \epsilon_0 \epsilon_{i2}}{\ln \left(\frac{r_5}{r_4} \right)} \right), \quad (24)$$

$$Y_{a4} = \left(\frac{j\omega 2\pi \varepsilon_0 \varepsilon_{i3}}{\ln \left(\frac{r_7}{r_6} \right)} \right). \quad (25)$$

Potential coefficients are inversely related to admittances [1]:

$$[P_i] = \begin{bmatrix} P_c + P_s + P_a & P_s + P_a & P_a \\ P_s + P_a & P_s + P_a & P_a \\ P_a & P_a & P_a \end{bmatrix}, \quad (26)$$

with:

$$P_c = \frac{j\omega}{Y_{cs}}, \quad (27)$$

$$P_s = \frac{j\omega}{Y_{sa}}, \quad (28)$$

$$P_a = \frac{j\omega}{Y_{a4}}. \quad (29)$$

2.3. Representation of a line by the chain matrix ϕ

2.3.1. Representation of a single-wire line

The telegraphic equations for a single-wire line (developed from the Maxwell equations) are [1]:

$$\frac{d^2 U(y)}{dy^2} = ZYU(y), \quad (30)$$

$$\frac{d^2 I(y)}{dy^2} = YZI(y). \quad (31)$$

The resolution of Eqs. (30), (31) in frequency gives us:

$$\begin{cases} U(y) = Ae^{-\gamma y} + Be^{+\gamma y} \\ I(y) = \frac{1}{Z_c} (Ae^{-\gamma y} - Be^{+\gamma y}) \end{cases}, \quad (32)$$

$$\gamma = \sqrt{ZY}, \quad (33)$$

such as:

$Ae^{-\gamma y}$: the incident wave,

$Be^{+\gamma y}$: the reflected wave,

A, B : integration constants, determined taking into account the boundary conditions as follows:

$$\begin{cases} U(y=0) = U_s \\ I(y=0) = I_s \end{cases}, \quad (34)$$

$Z_c = \sqrt{\frac{Z}{Y}}$: characteristic impedance,

$\gamma = \sqrt{ZY}$: exponent of propagation.

After a mathematical development we get the voltage and current equations based on the variable's space "y" along the length of the line, exposing gamma propagation and the quantities of entries [2].

$$\begin{cases} U(y) = \cosh(\gamma y) U_s Z_c \cdot \sinh(\gamma y) I_s \\ I(y) = \frac{\sinh(\gamma y)}{Z_c} U_s + \cosh(\gamma y) I_s \end{cases} \quad (35)$$

These last two expressions allow us to calculate the current and voltage values at any point of the line (Fig. 4). The system in matrix form is then written as

$$\begin{bmatrix} U(y) \\ I(y) \end{bmatrix} = [\phi] \begin{bmatrix} U_s \\ I_s \end{bmatrix}, \quad (36)$$

with the chain matrix for the single-wire line

$$\phi = \begin{bmatrix} \cosh(\gamma y) & Z_c \cdot \sinh(\gamma y) \\ -\frac{\sinh(\gamma y)}{Z_c} & \cosh(\gamma y) \end{bmatrix}. \quad (37)$$

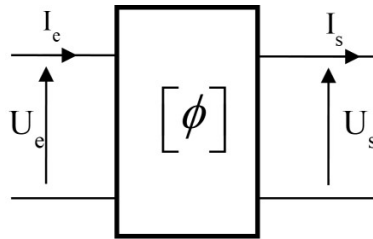


Fig. 4. Quadrupole representation by matrix $[\phi]$ of a single-wire line

2.3.2. Representation of a multi-wire line by the chain matrix ϕ

The cable is considered to be a multi-wire line. The equations of the line describing all drivers Fig. 1 (Eq. (1)) [2].

After some mathematical manipulations, we deduce the two telegraphic equations for a multi-wire line

$$\begin{cases} \frac{d^2 [\underline{U}(y)]}{dy^2} = [\underline{Z}] [\underline{Y}] [\underline{U}(y)] \\ \frac{d^2 [\underline{I}(y)]}{dy^2} = [\underline{Y}] [\underline{Z}] [\underline{I}(y)] \end{cases}, \quad (38)$$

with

$[\underline{U}(y)]$: voltage matrix a multi-wire line,

$[\underline{I}(y)]$: current matrix a multi-wire line.

$[\underline{Z}]$ and $[\underline{Y}]$, are respectively, the matrices of linear impedance and admittance of the multi-wire line.

2.3.3. Representation by the multi-pole chain matrix ϕ

In our study, we are interested in the values of voltages and currents at the ends of each tube (multilayer cable), these values can be linked by the chain matrix $\phi(L)$ as the following [1, 2]:

$$\begin{bmatrix} [\underline{U}(L)] \\ [\underline{I}(L)] \end{bmatrix} = \underline{\phi}(L) \begin{bmatrix} [\underline{U}(0)] \\ [\underline{I}(0)] \end{bmatrix} = \begin{bmatrix} \underline{\phi}_{11}(L) & \underline{\phi}_{12}(L) \\ \underline{\phi}_{21}(L) & \underline{\phi}_{22}(L) \end{bmatrix} \begin{bmatrix} [\underline{U}(0)] \\ [\underline{I}(0)] \end{bmatrix}, \quad (39)$$

or $\underline{\phi}_{ij}(L)$: under matrix of order n .

With the evaluation of $[\underline{U}(y)]$ et $[\underline{I}(y)]$, $y = 0$ and $y = L$, and eliminating $[\underline{I}_m^\pm]$ we get $[\underline{\phi}_{ij}(L)]$.

$$[\underline{\phi}_{11}(L)] = \frac{1}{2} [\underline{Y}]^{-1} [\underline{T}] \left(e^{+\underline{\gamma}_m L} + e^{-\underline{\gamma}_m L} \right) [\underline{T}]^{-1} [\underline{Y}], \quad (40)$$

$$[\underline{\phi}_{12}(L)] = -\frac{1}{2} [\underline{Y}]^{-1} [\underline{T}] \underline{\gamma}_m \left(e^{+\underline{\gamma}_m L} - e^{-\underline{\gamma}_m L} \right) [\underline{T}]^{-1}, \quad (41)$$

$$[\underline{\phi}_{21}(L)] = -\frac{1}{2} [\underline{T}] \left(e^{+\underline{\gamma}_m L} - e^{-\underline{\gamma}_m L} \right) \underline{\gamma}_m^{-1} [\underline{T}]^{-1} [\underline{Y}], \quad (42)$$

$$[\underline{\phi}_{22}(L)] = \frac{1}{2} [\underline{T}] \left(e^{+\underline{\gamma}_m L} + e^{-\underline{\gamma}_m L} \right) [\underline{T}]^{-1}, \quad (43)$$

The matrix $[\underline{T}]$ and the matrix $\underline{\gamma}$ are deduced by modal analysis [8].

$$\underline{\gamma}_m^2 = \begin{bmatrix} \underline{\gamma}_1^2 & 0 & \dots & \dots & 0 \\ 0 & \underline{\gamma}_2^2 & \dots & \dots & \dots \\ \dots & \dots & \underline{\gamma}_3^2 & \dots & \dots \\ \dots & \dots & \dots & \dots & 0 \\ \dots & \dots & \dots & \dots & \underline{\gamma}_n^2 \end{bmatrix}, \quad (44)$$

where T is a matrix of size $N \times N$ defined such that it diagonalizes the matrix $[YZ]$, that is verifying the relation $T^{-1} [ZY] T = [\underline{\gamma}_m]^2$. $\underline{\gamma}_m$ represents the diagonal matrix of squared propagation constants.

2.4. System construction $[A] [X] = [B]$

The topological formalism that we will expose is that proposed by A. Amétani *et al.* [1]. This formalism makes it possible to model the propagation of harmonic currents in a mesh or radial network of tubes (multi-wire line or multi-layer cable) (Fig. 5).

2.5. Principle of the analysis

The principle of the analysis consists in separating the propagating networks (tubes) from the localized networks (nodes and junctions). This resolution allows us to deduce all the currents and voltages on all the nodes (junction and end node) of the network, and thus to analyze the transfer function between the input and output (Fig. 6).

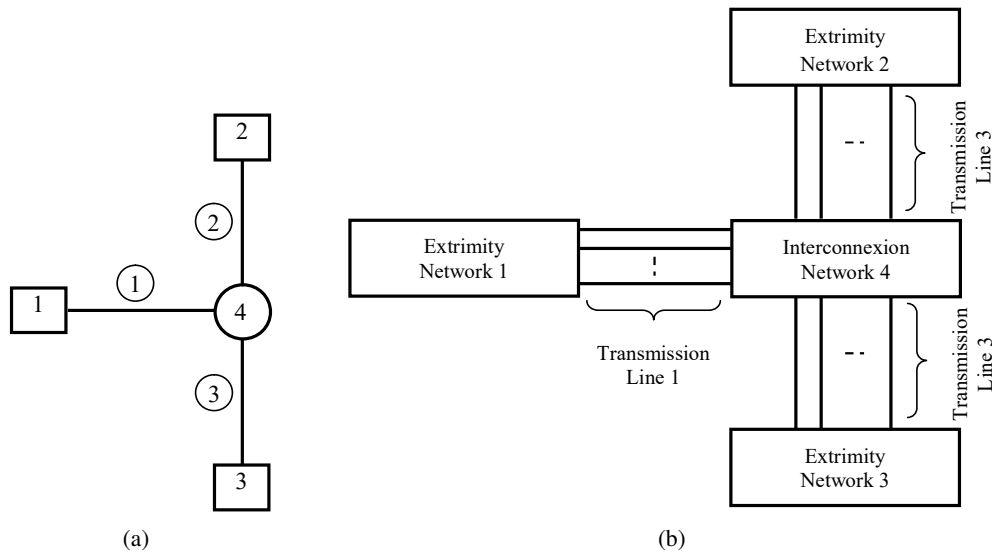


Fig. 5. Illustration of transmission lines network: (a) representation by a graph; (b) definitions of a tube and a network

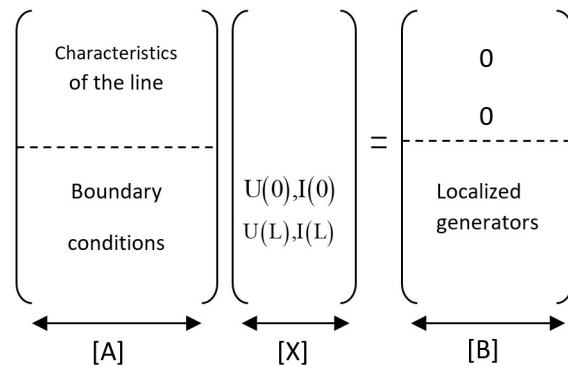


Fig. 6. Propagating networks and the localized networks

This approach will allow us to define the matrix $[A]$ composed of two sub-matrices [3].

$[A] = \begin{bmatrix} [A_1] \\ [A_2] \end{bmatrix}$ is the network topology representation matrix.

$[A_1]$ is the sub matrix deduced from all matrix representations of all the tubes in the network.

$[A_2]$ is the sub matrix deduced from Kirchhoff's laws for junctions and terminations nodes.

Once the matrix $[A]$ has been constructed, the resolution of the system of equations $[A][X] = [B]$ allows us to deduce the electrical quantities sought.

There, $[X]$ is the vector of the unknowns (currents and voltages on all the nodes) and $[B]$ is the source vector.

2.5.1. Sub-matrix of the tubes $[A_1]$

The sub-matrix defines the propagation on each of the tubes, and is given by the following equation:

$$[1_{2N}] \begin{bmatrix} [\underline{U}(L)] \\ [\underline{I}(L)] \end{bmatrix} - \begin{bmatrix} [\varphi_{11}(L)] & [\varphi_{12}(L)] \\ [\varphi_{21}(L)] & [\varphi_{22}(L)] \end{bmatrix} \begin{bmatrix} [\underline{U}(0)] \\ [\underline{I}(0)] \end{bmatrix} = \begin{bmatrix} 0 \\ 0 \end{bmatrix}. \quad (45)$$

This approach makes the elements of the matrix Φ appear directly in the sub-matrix $[A_1]$. $[A_1]$ contains all the data relating to the L multi-wire lines.

2.5.2. Sub-matrix of junctions $[A_2]$

The sub-matrix corresponds to the representations of all the nodes (end and interconnection networks) of the transmission network. This sub-matrix is obtained by applying the theorems of Thévenin and Norton in each node with

$$[A_2] = \begin{bmatrix} \text{Network}_i & & 0 \\ & \text{Network}_j & \\ 0 & & \text{Network}_k \end{bmatrix}. \quad (46)$$

Suppose, for example, that we want to characterize the interconnection network ‘ m ’, which performs the interconnection of the three tubes: i , j and k , as illustrated in Fig. 7.

The combination of Kirchhoff’s laws in voltage and current allow us to describe:

$$\sum_{l=1}^{NT} ([\underline{Y}_l^m] [\underline{U}_l^m] + [\underline{Z}_l^m] [\underline{I}_l^m]) = [\underline{P}^m], \quad (47)$$

where:

$[\underline{U}_l^m]$, $[\underline{I}_l^m]$ and $[\underline{P}^m]$ are of dimension NT , they represent, respectively, the vectors of voltages and currents at the input and output of the network and the generators of voltages and /or currents located at the network level,

$[\underline{Y}_i^m]$, $[\underline{Y}_j^m]$, $[\underline{Y}_k^m]$, $[\underline{Z}_i^m]$, $[\underline{Z}_j^m]$, $[\underline{Z}_k^m]$ are, respectively, the admittances, impedances are obtained by writing the equations of the meshes and of the nodes for the multi-pole l .

$[A_2]$ contains all the data relating to the m networks.

2.5.3. The vector $[B]$

This vector is composed of two sub-vectors $[0]$ and $[B_1]$, such as

$$[B] = \begin{bmatrix} [0] \\ [B_1] \end{bmatrix}. \quad (48)$$

The second sub-vector $[B_1]$ contains the generators located at each node (of voltages and/or currents), that is to say it includes the second members of the combination (48) written for each network m .

$$[B_1] = \begin{bmatrix} \vdots \\ [P^m] \\ \vdots \end{bmatrix}. \quad (49)$$

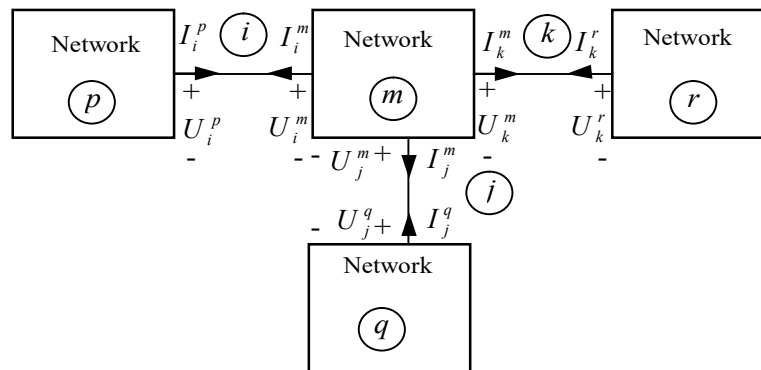


Fig. 7. Illustration of a junction node

3. CST software

Computer Imulation Technology software is a specialist tool for the tridimensional electromagnetic simulation of high frequency components. The software code is based on the integral method [16–19]. The choice of this software is for the calculation of the voltage transfer function which translates the relationship between the output voltage and the input voltage of the core ($TF = V(L)/V(0)$) in a broad frequency band [20].

The Computer Imulation Technology settings are used in all simulations, and the technique is FIT in time-domain. The version is CST EMC Studio-2017. It should be noted that all simulations were made using an Intel Core i7 2.60 GHz processor with 16 GB RAM.

4. Results and application

4.1. Physical and geometric parameters of the cable

The physical and geometric data used to perform the different applications, proposed in this paper, are shown in Fig. 8 below.

There: $r_1 = 1$ cm, $r_2 = 1.34$ cm, $r_3 = 1.48$ cm, $r_4 = 1.64$ cm, $r_5 = 1.81$, and $r_6 = 2$ cm. The electrical conductivity of the ground is $\sigma_{sol} = 0.01 \frac{S}{m}$.

4.2. Validation of results

4.2.1. Validation of the self-internal impedance of the core

The first validation concerns the proper internal impedance of the core (without taking into account the effect of the ground); we compare our results with those published by Amétani [1], (Fig. 9). There:

$N_C = 1(c)$: single-layer cable (core and its insulation),

$N_C = 2(b)$: cable made up of two conductive layers (core, screen) and their insulators,

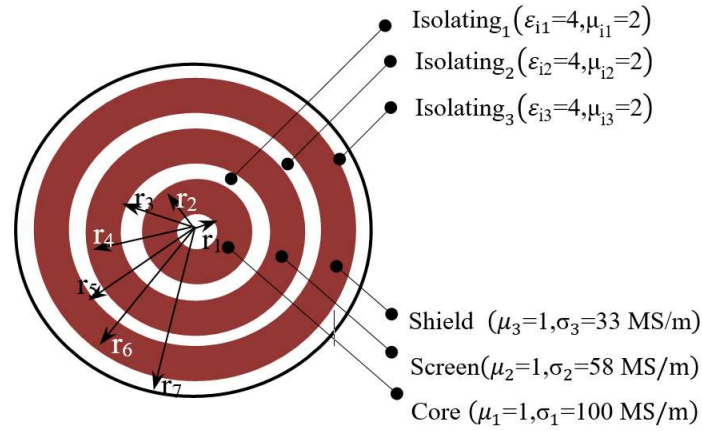


Fig. 8. Cross section of a coaxial cable

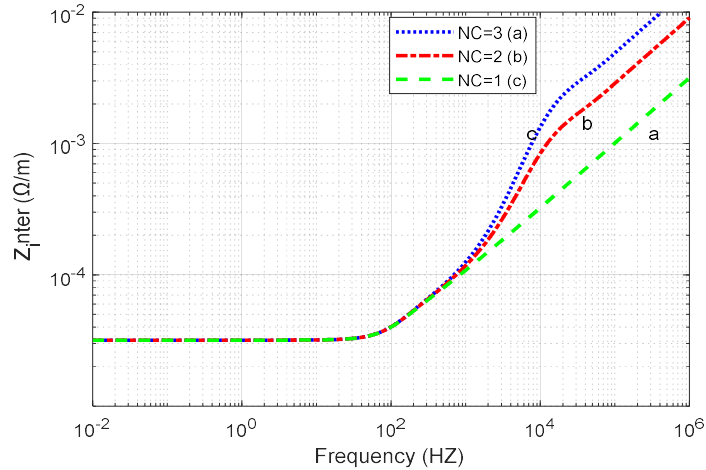


Fig. 9. Z-inter of a single core cable for different layers

$N_C = 3(a)$: cable made up of three conductive layers (core, screen, shielding) and their insulation.

4.2.2. Verification of the present method

For verifying the present method, the results of analytical method are compared with the results given by the simulation with the CST software (FIT). The buried cable was tested in this part with the frequency variation of the voltage transfer function which translates the relationship between the output voltage and the input voltage of the core ($TF = V(L)/V(0)$), and for a suitable cable ($Z = Z_c$).

According to Fig. 10, we notice that the results obtained by the numerical method (FIT), and those obtained by the analytical model are in good agreement.

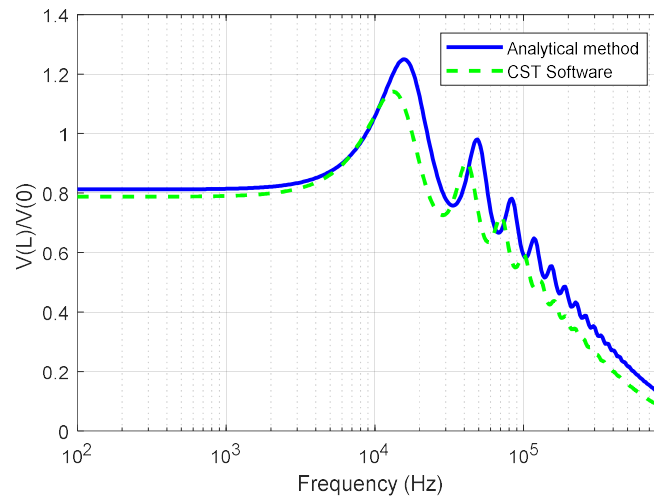


Fig. 10. The comparison result of the tension ratios ($V(L)/V(0)$) between circuital approach and CST software

Examination of the different curves obtained by the two methods with more than precision, allowed us to note the existence of a slight difference in terms of amplitudes of the resonant frequencies. This difference in levels can be explained by the following points:

The fact that the programmed numerical and analytical methods are based on certain approximate assumptions, unlike the CST software which is based on the method FIT and solves Maxwell's equations directly without neglecting any approximation.

4.3. Analysis of the propagation of HF signals over a single cable

The first part of the applications concerns the case of a simple cable with two end networks; in this part we are interested in the frequency variation of the voltage transfer function which translates the relationship between the output voltage and the input voltage of the core ($TF = V(L)/V(0)$). We will respectively analyze the effect and the influence of several factors on the transfer function such as: effect of an installation method, effect of end loads, cable length and the junction between two sections of cables.

4.3.1. Effect of installation method

Consider the two configurations representing two cables laid differently, the first is overhead and the second is buried for $Z = 10 \Omega$.

From the result in Fig. 11 below, we deduce that the transfer function is the same for both the aerial cable and the buried cable with the exception of a very slight difference at low frequencies.

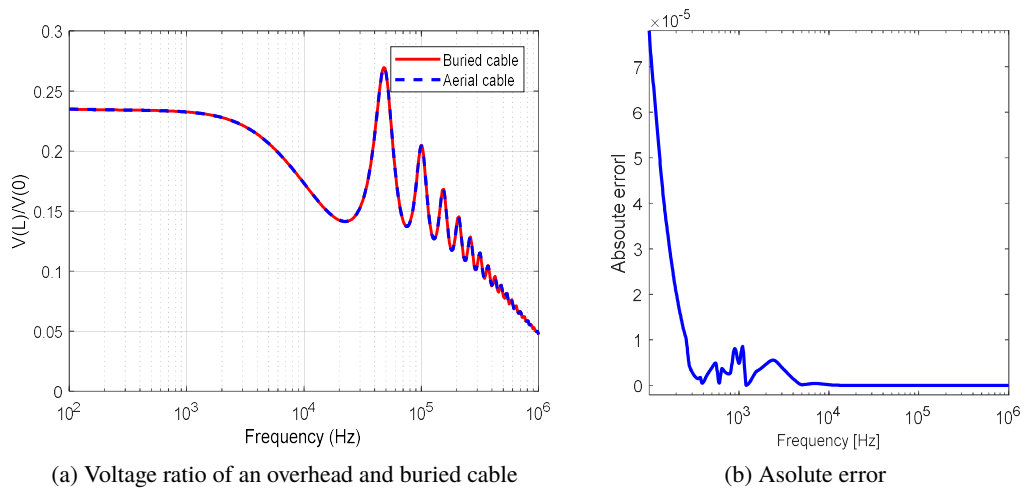


Fig. 11. Voltage ratio on the core of an over head and buried cable and absolute error of the difference between us for all frequencies

4.3.2. Effect of end loads

Either the configuration in Fig. 8, representing a buried cable, with the screen and the shield in short circuit and the core charged by an impedance Z .

By putting the screen and the shielding in short circuit on both sides of the cable, we note in Fig. 12 that the increase in the load of the core causes an improvement of the transfer function in amplitude while keeping the same resonances and the same optimal signal transmission bands.

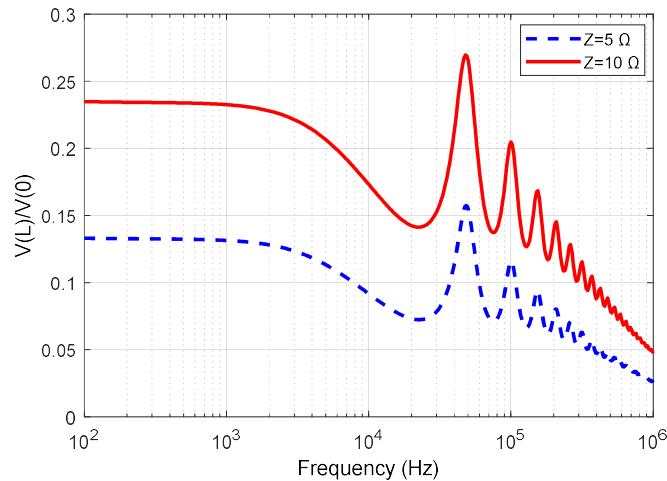


Fig. 12. Voltage ratio with the variation of the end load of the core

4.3.3. Effect of cable length

Keeping the same configuration as above Fig. 8 we simulate the propagation of the signals on three cables of different lengths ($Z = 10$).

From the results in Fig. 13, we note that the transfer function is strongly linked to the length of the cable; which is to be expected because on the one hand the transfer function will depend on the ratio between the length of the cable and that of the wavelength as well as on the attenuation of the signal which is linked to the distance traveled and therefore increases with the length. Note also that the resonant frequencies are now shifted, which translates into a difference in the transmission channel.

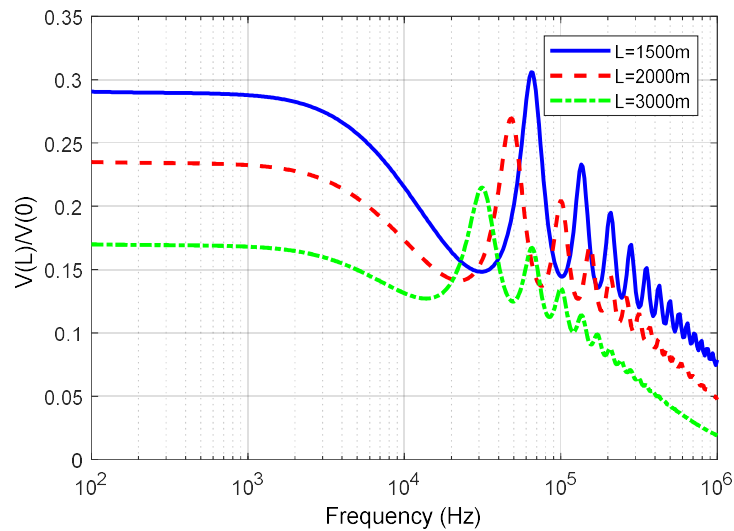


Fig. 13. The effect of varying the length

4.3.4. Effect of the junction between two cable sections

The goal is to show the effect of a discontinuity on the propagation.

The presence of a junction in the cable highlights the appearance of attenuation on the transfer function over the entire frequency range and causes the disappearance of certain resonance frequencies; this last point can be explained by the appearance of signal reflection phenomena at the junction unlike the direct cable which causes a change in resonance frequencies (Fig. 14).

4.4. Analysis of the propagation of HF signals over a cable network in T

As a second type of application, we propose to treat propagation in the case of a T-shaped network made up of three cables of the same length (L) and a junction as shown in Fig. 5. The analysis will focus on the variations of the transfer function.

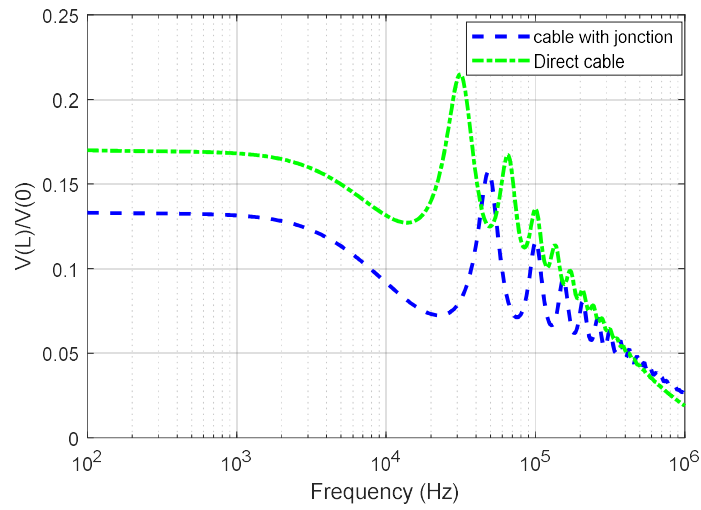


Fig. 14. Effect of the presence of a junction

4.4.1. Effect of end loads ($l = 1000$ m, $Z_2 = 100 \Omega$, $Z_3 = 200 \Omega$)

Either the configuration in Fig. 5, where we have a T-shaped network made up of three cables (tubes); initially at the signal injection end we consider the case where the screen and the shield are grounded.

From the results in Fig. 15, we can easily see that the highest load leads to a better amplitude transfer function.

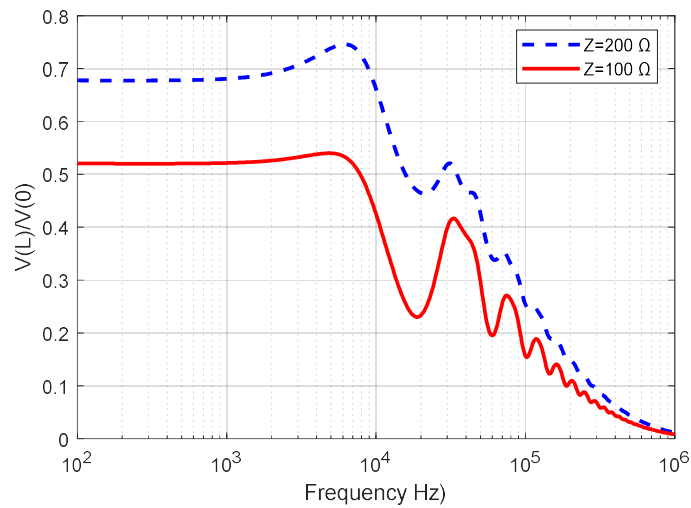


Fig. 15. Effect of the end load of a T network

4.4.2. Effect of screen connection mode and network shielding 1, 2 and 3

From the results in Fig. 16, we note that the grounding of screens and shields for all localized networks leads to a better-quality transfer function; we note indeed that the amplitude is greater and the transmission channel is much wider with fewer resonant frequencies.

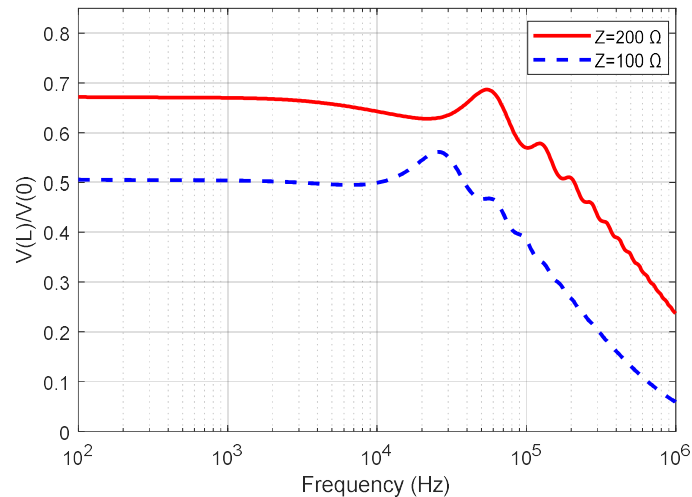


Fig. 16. Effect of short circuit

These results clearly show that the grounding of screens and shields for all localized networks leads to a better-quality transfer function; we note indeed that the amplitude is greater and the transmission channel is much wider with fewer resonant frequencies.

5. Conclusion

In this work, we approach the propagation of the HF signals as well on a simple cable as on a topology in T. We look more particularly at the effect of a junction, the connection mode of the screen and the shielding, and the cable length on the transfer function between the input and the output of the cable. We can also say that all the results clearly confirm the choice currently used for the frequency range up to 400 kHz; indeed, our simulation results clearly show that in this range there is an absence of resonances, therefore possible signal cutoff. The PLC system is an effective means of transmitting information via power cable for utilization in power stations. However, the reservations made by the channel being the power line in terms of bandwidth is low. In addition, with the advancements of networking and information technology and other communications modes, there is a need for development in the power line carrier system to enable the transfer of a large amount of information at a specified bit rate possible. The traditional PLC system for control and communication purposes is still widely revered in power systems despite other advancements in communication modes; it remains highly reliable in issuing control commands to power systems equipment.

Acknowledgements

This work is supported by the General Directorate of Scientific Research and Development Technological (DGRSDT).

References

- [1] Amétani A., *A General Formulation of Impedance and Admittance of Cables*, IEEE Transactions on Power Apparatus and Systems, vol. Pas-99, no. 3, pp. 902–910 (1980), DOI: [10.1109/TPAS.1980.319718](https://doi.org/10.1109/TPAS.1980.319718).
- [2] Haotian Ge, Bingyin Xu, Wengang Chen, Xinhui Zhang, Yongjian Bi, *Topology identification of low voltage distribution network based on current injection method*, Archives of Electrical Engineering, vol. 70, no. 2, pp. 297–306 (2021), DOI: [10.24425/ae.2021.136985](https://doi.org/10.24425/ae.2021.136985).
- [3] Besnier P., *Etude des couplages électromagnétiques sur les réseaux de lignes de transmission non uniformes à l'aide d'une approche topologique*, PhD Thesis, Department of Electronics, Université de Lille (1993).
- [4] Rouissi F., Vinck A.J.H., Gassara H., Ghazel A., *Improved impulse noise modeling for indoor narrow-band power line communication*, AEU - International Journal of Electronics and Communications, vol. 103, no. 1, pp. 74–81 (2019), DOI: [10.1016/j.aeu.2019.02.019](https://doi.org/10.1016/j.aeu.2019.02.019).
- [5] Rastislav R., *Experimental measurements for evaluation of the network throughput of the RC4 channel in the in-home PLC network*, Journal of Electrical Engineering, vol. 70, no. 1, pp. 25–31 (2019), DOI: [10.2478/jee-2019-0003](https://doi.org/10.2478/jee-2019-0003).
- [6] Meng H., Chen S., Guan Y.L., Law C.L., So P.L., Gunawan E., Lie T.T., *Modeling of transfer characteristics for the broadband power line communication channel*, IEEE Transactions on Power Delivery, vol. 19, no. 3, pp. (2004), DOI: [10.1109/TPWRD.2004.824430](https://doi.org/10.1109/TPWRD.2004.824430).
- [7] Sykora T., Husak M., Bastan O., Benes T., *Automatic generation of a PLC controller based on a control system-identified model*, Journal of Electrical Engineering, vol. 72, no. 2, pp. 78–88 (2021), DOI: [10.2478/jee-2021-0011](https://doi.org/10.2478/jee-2021-0011).
- [8] Adesina L.M., Abdulkareem A., Ogunbiyi O., *Effects of Ground Resistivity and Tower Structural Design on Transmission Line Symmetrical Components*, International Journal of Recent Technology and Engineering (IJRTE), vol. 9, no. 1, pp. 2115–2126 (2020), DOI: [10.35940/ijrte.A2519.059120](https://doi.org/10.35940/ijrte.A2519.059120).
- [9] Xiao Z., *Power communication network design considering global information fusion part two applications and explorations*, Procedia Computer Science, vol. 155, no. 3, pp. 768–773 (2019), DOI: [10.1016/j.procs.2019.08.112](https://doi.org/10.1016/j.procs.2019.08.112).
- [10] Shekoni O.M., Hasan A.N., Shongwe T., *Applications of artificial intelligence in power line communications in terms of noise detection and reduction*, Aust. J. Electr. Electron. Eng., vol. 15, no. 1–2, pp. 29–37 (2018), DOI: [10.1080/1448837X.2018.1496689](https://doi.org/10.1080/1448837X.2018.1496689).
- [11] Potisk L., Hallon J., Orgon M., Fujdiak R., *Electromagnetic compatibility of PLC adapters for in-home/domestic networks*, Journal of Electrical Engineering, vol. 69, no. 1, pp. 79–84 (2018), DOI: [10.1515/jee-2018-0011](https://doi.org/10.1515/jee-2018-0011).
- [12] Sharma D., Dubey A., Mishra S., Mallik R.K., *A Frequency Control Strategy Using Power Line Communication in a Smart Microgrid*, IEEE Access, vol. 7, no. 1, pp. 21712–21721 (2019), DOI: [10.1109/ACCESS.2019.2897051](https://doi.org/10.1109/ACCESS.2019.2897051).
- [13] Henryk S., Lerch B., Bień A., *Monitoring of PV Inverters while Unintentional Islanding Using PMU*, International Journal of Electronics and Telecommunications, vol. 67, no. 3, pp. 465–470 (2021), DOI: [10.24425/ijet.2021.137835](https://doi.org/10.24425/ijet.2021.137835).

- [14] Mahmood S.H., Salih A.M., Khalil M.I., *Broadband services on power line communication systems*, 22nd International Conference on Control Systems and Computer Science (CSCS), pp. 465–470 (2019), DOI: [10.1109/CSCS.2019.00085](https://doi.org/10.1109/CSCS.2019.00085).
- [15] Cano C., Pittolo A., Malone D., Lampe L., Tonello A.M., Dabak A.G., *State of the Art in Power Line Communications: From the Applications to the Medium*, IEEE Journal on Selected Areas in Communications, vol. 34, no. 7, pp. 1935–1952 (2016), DOI: [10.1109/JSAC.2016.2566018](https://doi.org/10.1109/JSAC.2016.2566018).
- [16] Wolkerstorfer M., Schweighofer B., Wegleiter H., Statovci D., Schwaiger H., Lackner W., *Measurement and simulation framework for throughput evaluation of narrowband power line communication links in low-voltage grids*, Journal of Network and Computer Applications, vol. 59, no. 2, pp. 285–300 (2016), DOI: [10.1016/j.jnca.2015.05.022](https://doi.org/10.1016/j.jnca.2015.05.022).
- [17] Andreadou N., Fulli G., *NB-PLC channel: Estimation of periodic impulsive noise parameters and mitigation techniques*, International Journal Electrical Power and Energy Systems, vol. 103, no. 2, pp. 146–158 (2019), DOI: [10.1016/j.ijepes.2018.05.011](https://doi.org/10.1016/j.ijepes.2018.05.011).
- [18] Korecki J., Menach Y., Ducreux J., Piriou F., *Numerical solutions in primal and dual mesh of magnetostatic problem solved with the Finite Integration Technique*, Compel, vol. 27, no. 1, pp. 47–55 (2008), DOI: [10.1108/03321640810836627](https://doi.org/10.1108/03321640810836627).
- [19] Albertier G., Le Menach Y., Ducreux J.P., Piriou F., *Consideration of the coupling of magnetic and electric equations with Finite Integration Technique (FIT)*, European Physical Journal, Applied Physics, vol. 30, no. 1, pp. 17–22 (2005), DOI: [10.1051/epjap:2005018](https://doi.org/10.1051/epjap:2005018).
- [20] Ling Liu X.C., *Design of broadband power line communication module for automatic meter reading*, Archives of Electrical Engineering, vol. 69, no. 4, pp. 771–780 (2020), DOI: [10.24425/ae.2020.134628](https://doi.org/10.24425/ae.2020.134628).